The Radio Luminosity Function and Galaxy Evolution of Abell 2256

A THESIS
SUBMITTED TO THE FACULTY OF THE GRADUATE SCHOOL
OF THE UNIVERSITY OF MINNESOTA
BY

Zahra Forootaninia

IN PARTIAL FULFILLMENT OF THE REQUIREMENTS
FOR THE DEGREE OF
MASTER OF SCIENCE

Lawrence Rudnick, Advisor

January, 2015

Acknowledgements

I would like to express my special appreciation and thanks to my advisor Professor Lawrence Rudnick who has been a good mentor and gave me the unique opportunity and support. I appreciate his guidance, generous contribution of knowledge and experience and valuable comments in my search.

I would also like to thank my committee members, Professor Terry Jones, Professor Robert Lysak and Professor Thomas Jones for serving as my committee members even at hardship.

I would especially like to thank Professor Frazer Owen at National Radio Astronomy Observatory, for providing me with very fascinating data and his brilliant comments, suggestions and help.

Next, I would like thank to Dr Kyle Willett for being so generous in sharing his knowledge and time with me. His recommendations always helped me find the correct path in my research. Also, I would like to thank Dr Reinout van Weeren for allowing me to use his Hubble Space Telescope data.

A special thanks to my family. Words cannot express how grateful I am to my mother, father and my sister for all of the sacrifices that they have made on my behalf. I would also like to thank all of my friends who supported me in writing, and incited me to strive towards my goal. At the end, I would like express my appreciation to Mehdi Lamee who spent sleepless nights with me, and has always supported me in the moments when there was no one to answer my queries.

Dedication

I dedicate my thesis to my parents. This accomplishment was only possible due to their love and sacrifices. Without them none of this would be possible.

Abstract

This thesis presents a study of the radio luminosity function and the evolution of galaxies in the Abell 2256 cluster (z=0.058, richness class 2). Using the NED database and VLA deep data with an rms sensitivity of 18μ Jy.$beam^{-1}$, we identified 257 optical galaxies as members of A2256, of which 83 are radio galaxies. Since A2256 is undergoing a cluster-cluster merger, it is a good candidate to study the radio activity of galaxies in the cluster.

We calculated the Univariate and Bivariate radio luminosity functions for A2256, and compared the results to studies on other clusters. We also used the SDSS parameter fracDev to roughly classify galaxies as spirals and ellipticals, and investigated the distribution and structure of galaxies in the cluster.

We found that most of the radio galaxies in A2256 are faint, and are distributed towards the outskirts of the cluster. On the other hand, almost all very bright radio galaxies are ellipticals which are located at the center of the cluster. We also found there is an excess in the number of radio spiral galaxies in A2256 compared to the number of radio ellipticals, counting down to a radio luminosity of $log(luminosity) = 20.135$ W/Hz.

Contents

List of Tables

List of Figures

Chapter 1

Introduction

Abell 2256 is a massive galaxy cluster ($M \sim 10^{15} M_{\odot}$) of richness class 2, with a redshift $z = 0.058$ and with an X-ray luminosity 10^{40} to 10^{41} ergs/s (Sun et al. [2002]). Previous studies identified ~ 40 radio galaxies as members of the cluster (Miller et al. [2003b]). Berrington et al. [2002] proposed that A2256 contains three merging subclusters. Two of them appear to be at the advanced stage of the merging process, while the third subcluster is in the early stage of merging with the other two.

This unique merging environment of Abell 2256 makes it an interesting target to study the merging process and its effect on the intracluster medium (ICM) as well as the structure of galaxy clusters. For example, the origin of the observed diffuse emission (which extends for $\sim 1 Mpc$) from the cluster environment observed in radio (Miller et al. [2003b], Owen et al. [2014]) and X-ray (Clarke and Ensslin [2006]) is a subject of active research. There are two kinds of Mpc scale emission. First is the radio relic, which is diffuse emission that is distributed on the outskirts of the cluster with an irregular and elongated shape. Second is the radio halo emission which mostly originates from the center of clusters and has a similar morphology in both X-ray and radio. Figure 1.1 shows the radio relic and halo in Abell 2256 along with all cluster galaxy members. The source of these diffuse radio emissions are the relativistic particles that are generated by shocks created in the cluster merging process; seed relativistic particles may also be provided by the cluster radio galaxies. Simulations have shown that cluster-cluster mergers are a very energetic process, involving kinetic energies on the order of 10^{64} ergs. A fraction of this energy can be spent on stimulating the intra-cluster magnetic

field that accelerates relativistic particles, and produces diffuse synchrotron emission on large scales (Brunetti and Jones [2015]).

Cluster mergers can affect the environment and evolution of the individual galaxies in the cluster as well. There are two types of emission from galaxies we can see in the radio, emission from Active Galactic Nuclei (AGN) and Star Forming (SF) galaxies.

There are three main morphologies observed from radio galaxies: compact, extended, and jets/lobes. If the radio source is compact it is either an AGN or SF. If the radio source is extended and has the same size at its optical emission then the galaxy is SF.

It has been suggested that cluster merging can trigger star formation activities in galaxies. Merging increases the relative velocity between the galaxies and the velocity of the ICM. As a result, the ram-pressure applied by the ICM to the galaxy interstellar medium (ISM) increases and transfers gas to galaxy nuclei and enhances star formation. On the other hand, the ram pressure can also remove the ISM within the galaxies, decreasing star formation (see Ferrari [2005]).

Our understanding of cluster merging effects is incomplete, and even contradictory in some cases. While some observations such as Dressler et al. [1999] have shown that merger activities have a huge effect on the star formation rate within individual galaxies, other studies such as Yee et al. [1996] claim it does not play a significant role. Moreover, this contradiction extends to the available models and simulations as well. Fujita et al. [1999] showed that merger events can stop star formation in galaxies, while in the simulation by Fujita [1998] cluster merging enhances the star formation activity. These opposite results are mostly due to the different parameters that are assumed in different models and simulations.

AGNs can also be triggered by cluster merging. Gilmour et al. [2007] showed that there are fewer AGNs in the centers of cluster than outer regions. This could be due to the cold gas that is stripped away from ICM and there will be less fuel for AGNs in the cluster center (see Pimbblet et al. [2013]). Other studies show no effect of cluster merging on AGNs (examples are Haggard et al. [2010], Miller et al. [2003a]).

Studying the radio source and its optical counterpart in Abell 2256, as well as the distribution and structure of individual galaxies, and comparing these to other clusters may lead us to better understanding of the complex environment of merging clusters.

In this paper, we identify 83 radio objects as members of Abell 2256. We compute the Univariate and Bivariate Radio Luminosity Function (URLF and BRLF). The URLF gives us information about the distribution of radio luminosity of cluster member galaxies, while the BRLF is one of the best approaches towards understanding how optical magnitude affects the existence of radio emission . We also compared our result with the Coma cluster (Miller et al. [2009]), and the 188 galaxies in several Abell clusters (Ledlow and Owen [1996]). We used the Sloan Digital Sky Survey, SDSS, data release 10 to identify elliptical and spiral members of the cluster, which helped us to study and discuss their structure and distribution separately.

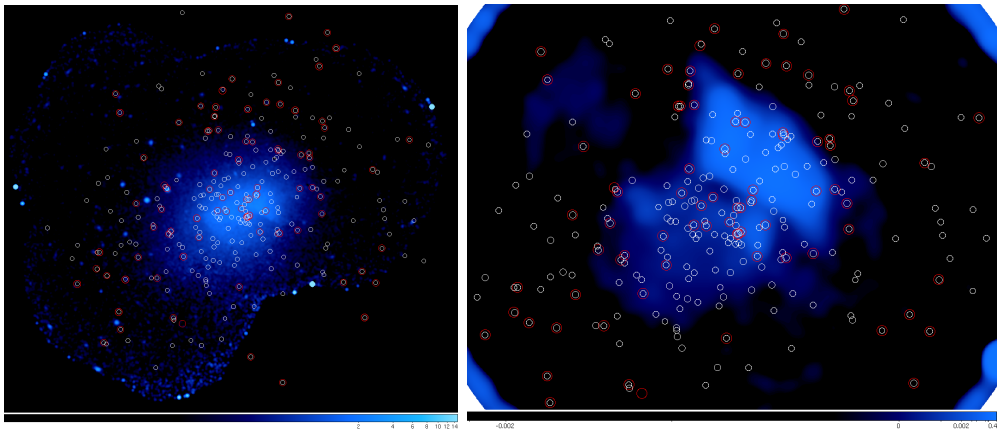

(a) Radio halo (b) Radio relic

Figure 1.1 Left: X-ray emission from the radio halo of A2256(in blue), Right: Radio emission from radio relic (in blue). White circles are optical galaxies in A2256 while red circles represent radio galaxy members.

Chapter 2

Radio and Optical Measured Quantities

In this chapter, we list and explain the quantities that we used for our analysis. Tables A.1 and A.2 list these calculated radio and optical quantities for the 85 radio sources in Abell 2256, of which we consider 83 to be reliable identification.

Data from Owen et al. [2014] were used to identify radio sources. These data have been observed with the Karl G. Jansky Very Large Array (VLA) at a frequency range of 1 GHz to 8 GHz; only the data at 1-2 GHz are used in this paper. These observations were obtained in all four VLA configurations (A,B,C and D). Owen et al. [2014] combined all four configurations to show both extended and compact structures in a single map. The final image is 0.41 degrees in radius with 3 arcsec resolution. This image is primary beam corrected, and therefore the noise level in the central regions is approximately 4 microJy while it increases to 26 microJy toward the edges.

Positions of the cluster members: We used the NASA/IPAC Extragalactic Database (NED) and looked for all the optical galaxies within the 0.41 degrees of the center of our radio map (RA=255.9317 deg , DEC=78.6666 deg). It should be noted that there is a 1.8 arcmin offset between the center of the radio and the X-ray maps. Note that if we change the center to the X-ray center, it will not affect our results. We only selected galaxies with spectroscopic redshifts of $0.047 \leq z \leq 0.069$, the same redshift range as Miller et al. [2003b]. Figure 2.1 shows the redshift distribution of all

galaxies within our search radius.

We selected 257 galaxies as cluster members of Abell 2256. We confirmed the NED coordinates of these galaxies by using the HST images kindly provided by van Weeren et al. [2009] (when available), and the SDSS DR10 catalog. It should be noted that we found two objects with SDSS ids of 1237663269868994575 and 1237663269332058258 where the optical positions were incorrect, but less than 4 arcsec off from the core of the galaxy, so we changed the optical positions to the correct ones. Figure 2.2 shows optical images of a few cluster members as an example. The radio intensity contours are plotted on top of the optical image, and the red cross represents the optical center of the galaxy.

We visually inspected and compared the radio and optical maps of the region, and found that 85 out of the 257 optical sources are associated with radio galaxies with a 4.5σ detection above the local background.The faintest optical galaxies have apparent magnitude of 22.16 and absolute magnitude of -14.81. However, the radio and optical centers of the two galaxies with SDSS IDs of 1237663269868929212 and 123766326933212388 do not match (you can see the images of these two objects in Chapter 7). Therefore, we decided not to include them in our sample for further analysis. The other 83 objects are classified as radio sources which belong to the Abell 2256 cluster.

Flux densities: We measured the peak and total flux densities of each galaxy member using the task "Viewer" from the Common Astronomy Software Applications (CASA) package. To measure the total flux densities, we manually drew a box around each object, and measured the total flux within the box, after removing any local background. In addition, we recorded the peak flux per beam for each object and made sure all radio sources had a peak flux above 4.5σ of the local background, which is 18 μJy at the center of the image, and increases to 116 μJy at the edge.

Luminosity: We calculated the luminosity of each galaxy from the measured total flux assuming all galaxies are located at the redshift of Abell 2256, $z = 0.058$, and Hubble parameter of $H_0 = 70 kms^{-1}Mpc^{-1}$.

Enclosed Area: Area enclosed by a circle which is centered on the cluster radio image and extending to the position of radio source.

Number of enclosed optical sources: Number of cluster optical galaxies within the enclosed area.

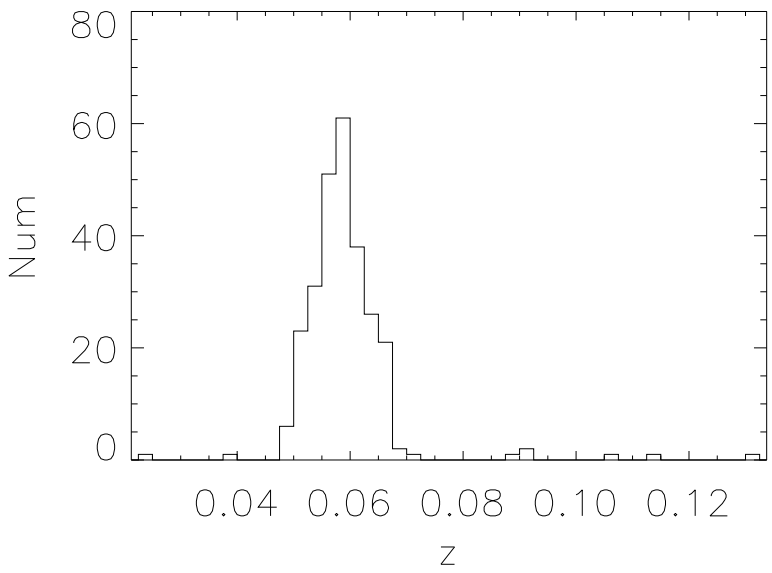

Figure 2.1 Redshift distribution of all galaxies found within 0.41 degrees of the radio center of the cluster, RA=255.9317 deg, DEC=78.6666 deg.

Sensitive Area: We defined the circular sensitive area as the region where a radio galaxy with its measured peak flux density could still be detected above 4.5σ. For example, a galaxy with the peak flux density of $18\mu Jy/beam$ could be detected above 4.5σ up to a radius of 0.49 Mpc from the center of the radio map.

Number of observable optical sources: Number of cluster optical galaxies in the sensitive area.

fracDev: This is a fractional parameter from the SDSS survey in different bands, which classifies galaxies as disk-like or elliptical, and can take values between 0 (for fully disk-like galaxies), and 1 (for fully elliptical galaxies). FracDev measures the ratio of the amount of estimated flux density by fitting two different surface brightness profiles, an exponential and a deVaucouleurs profile to the image of the galaxy. In this study, we used the SDSS r-band fracDev parameter. We will discuss this with more details in section 4.

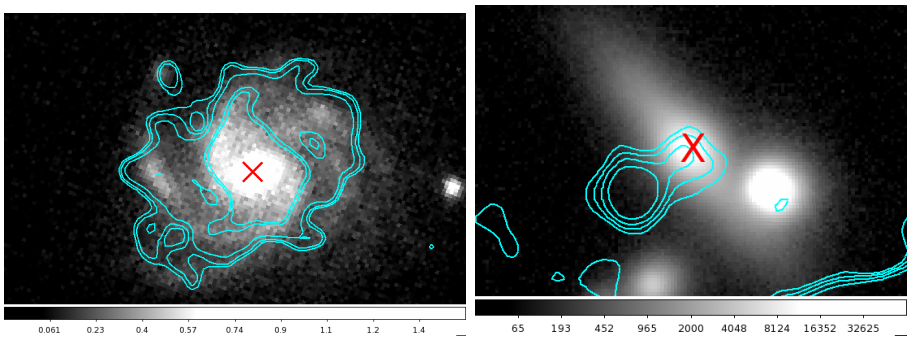

(a) $16:58:18.4, +78:29:34.1$ (b) $17:03:11.9, +78:40:30$

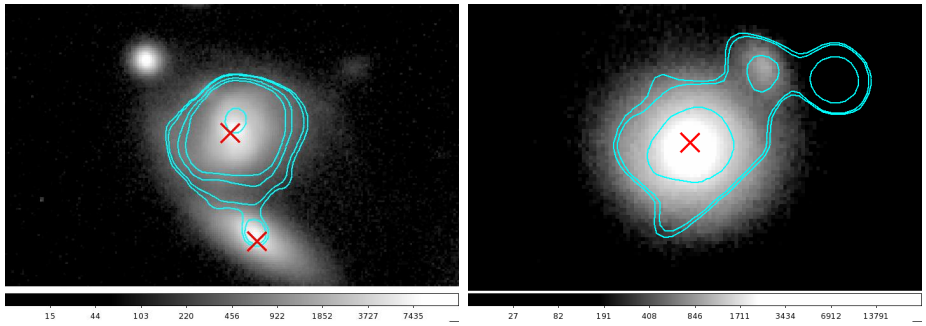

(c) $17:02:17.8, +78:45:51.8$ *and* $17:02:18.5, +78:46:04.1$ (d) $17:07:27, +78:36:20.8$

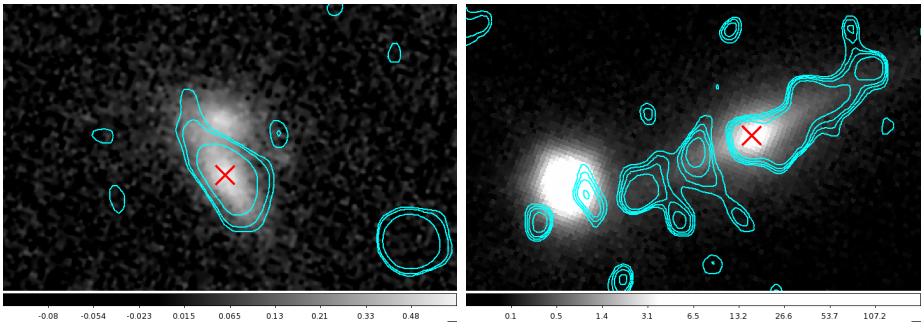

(e) $17:02:16.9, +78:54:11.2$ (f) $16:58:02.1, +78:33:48.1$

Figure 2.2 Example images of cluster members in optical with radio contours on the top. The red cross shows the center of the optical source we identified as the cluster member. Some of the optical images were kindly provided by van Weeren et al. [2009]

Chapter 3

Radio Luminosity Function

The shape of the Radio Luminosity Function (RLF) can tell us about the luminosity distribution of galaxies in Abell 2256 as well as the environment of the cluster. It also helps us understand the evolution of galaxies and the radio activity in the cluster. In the next two sections we calculate and discuss the RLF of Abell 2256, and compare it to the results from the Miller et al. [2009] work on the Coma cluster as well as Ledlow and Owen [1996] who studied a sample of different clusters.

There are several ways to characterize the luminosity function of radio sources in the cluster. We will use the following terminology in this paper:

- **Radio Luminosity Function(RLF)** The surface density of radio objects within the radio power bin. This is a classical version of the luminosity function which is similar to the definition of optical luminosity function (Mobasher et al. [2003]).
- **Univariate Radio Luminosity Function (URLF)** The sum of the number of radio sources in the observed bin of the radio power, divided by the total number of galaxies that could have been detected (as determined by the number of optical galaxies in the sensitive area for that bin) (Ledlow and Owen [1996]). The URLF can be interpreted as the probability for the members of the cluster to emit in the radio as shown in equation 3.1.

$$\phi(P) = \sum \frac{n(P_i)}{N(P_i)} \tag{3.1}$$

In this equation, $\phi(P)$ is the URLF, n is the number of radio sources in the radio power bin, P_i, and N is the number of galaxies that could have been detected. To measure N we count all the optical galaxy members in the sensitive area of the radio power bin.

- **Bivariate Radio Luminosity Function (BRLF)** The fraction of all galaxies with optical magnitudes between M and $M + dM$ and with radio power between P and $P + dP$. For comparison, the URLF is the sum over all magnitudes of the BRLF for a given radio power. Equation 3.2 from Ledlow and Owen [1996] shows the BRLF,

$$\phi(P, M) = \frac{n(P_i, M_i)}{N(P_i, M_i)} \tag{3.2}$$

$\phi(P, M)$ in this equation is the BRLF, $n(P_i, M_i)$ is the number of radio galaxies within the radio power bin P_i and the optical magnitude bin of M_i, and finally $N(P_i, M_i)$ is the number of detectable galaxies in the same optical and radio bin as $n(P_i, M_i)$.

In Figure 3.1 we plotted the RLF for A2256 (red line) and compared it to the Coma cluster (Miller et al. [2009], blue line). Assuming that all galaxies are at the same distance from us, we calculated the surface density of radio sources as a function of luminosity. To compare the calculated Abell 2256 RLF properly to the same quantity of the Coma cluster, we only used radio sources with maximum distance of 0.9 Mpc from the center of the Abell 2256 radio image. The radius 0.9 Mpc is used to sample the same area as the Coma cluster in Miller et al. [2009]. As can be seen from Figure 3.1, the Abell 2256 and Coma RLFs have a very similar shape up to the radius of 0.9 Mpc. This coincidence might be the result of the very similar environment of the two clusters.

Figure 3.2 shows the cumulative (integrated) URLF of A2256 (in black) and the URLF of the sample of 188 radio sources in the Abell clusters studied in Ledlow and Owen [1996] (in green). Their sample consist of radio galaxies with $z < 0.09$, Abell's distance class < 3 and integrated flux densities greater than 10 mJy at 20 cm. Ledlow and Owen [1996] studied the relationship of the radio and optical luminosities of radio

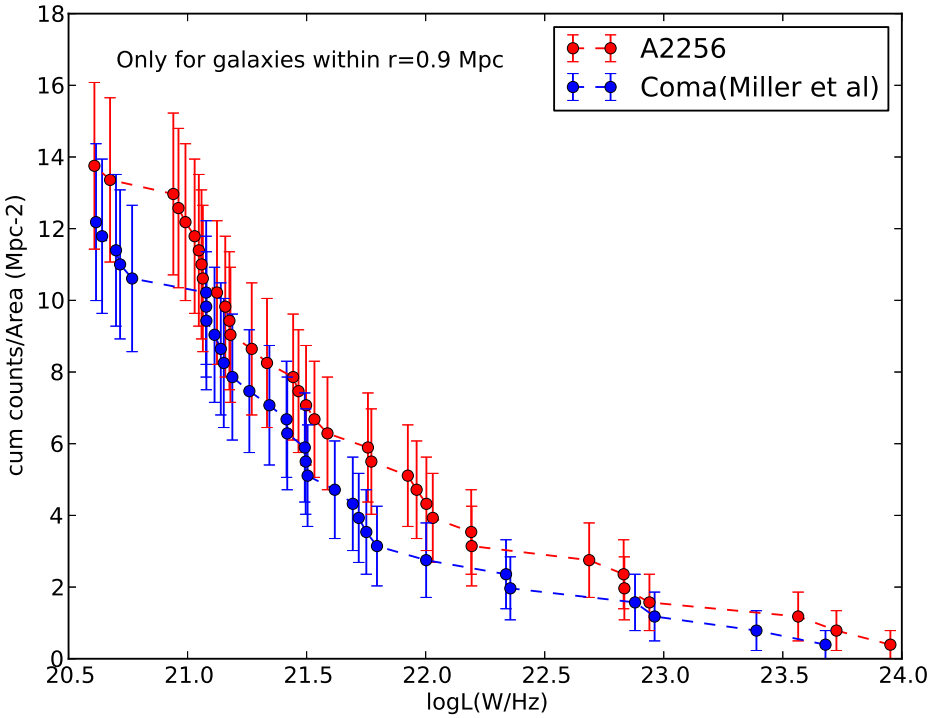

Figure 3.1 The cumulative Radio Luminosity Function for A2256 and the Coma cluster. The red line is the RLF of the A2256 while the blue line represents the Coma cluster from Miller et al. [2009] Figure 9.

sources in a sample of Abell clusters, and calculated the URLF and BRLF. They found that as the optical luminosity increased the probability of detecting radio sources went up as well.

As shown in Figure 3.2 the URLF of the galaxy sample from Ledlow and Owen [1996] is higher than A2256. We think this inconsistency is due to the different normalization methods used in calculating the URFL. Ledlow and Owen [1996] estimated the number of elliptical galaxies in the Abell surveyed radius for each cluster using the distribution and results from Dressler [1980]. Then they used the total number of ellipticals to normalize their URLFs. However, we used the number of observable optical sources (as previously defined) for each object as the total number of galaxies that could have been detected in radio. We used this number for the normalization of our URLFs. We

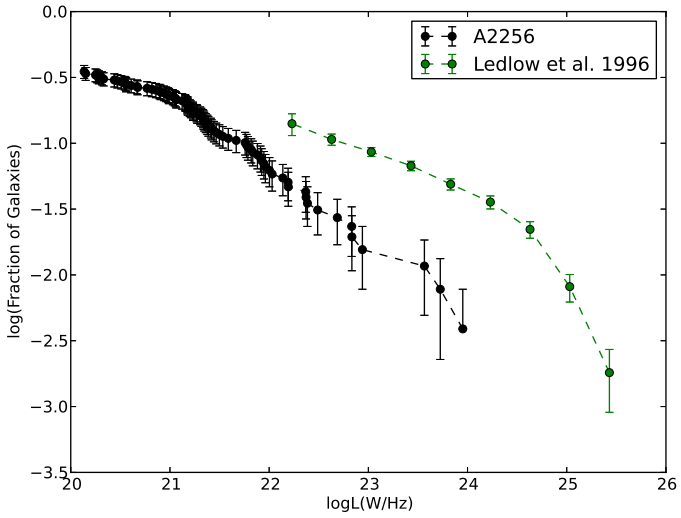

Figure 3.2 Cumulative Univariate Radio Luminosity Function. The green line shows the URLF of 188 sources listed in table A.2 from Ledlow and Owen [1996], and the black line is the URLF of A2256 calculated in this work. The excess in the green URLF is partially because Ledlow et al. normalized their URLF only by the elliptical galaxies that could have been detected while, we normalized by the number of all galaxies. Another major effect is that our counts of optical galaxies extended down to -14.81, while that for Ledlow and Owen are limited to -21.62.

used all kinds of galaxies for normalization rather than only ellipticals. Therefore, the denominator of our URLF goes up, and as a result our URLF is smaller. Another difference is that our absolute magnitude limit is -14.81 however the faintest galaxy in Ledlow et al. sample is -21.62, therefore we detected more optically faint galaxies than they did.

The URLF for A2256 increases to 35%. Most radio sources in Abell 2256 are faint. In fact, the fraction of faint galaxies in our sample is larger than in Ledlow and Owen [1996]. However, they found more luminous sources in their collection of radio galaxies compared to A2256. This is expected since most clusters do not have large number of luminous galaxies, but looking at a collection of galaxies from multiple clusters increases the probability of finding more luminous galaxies.

The more useful definition of the RLF is when we use both the radio power and the optical magnitude together for binning. This way we can simultaneously count galaxies

based on their optical and radio properties. Figure 3.3 shows the BRLF for three bins of optical magnitudes in r-band, -23.40 to -20.60, -20.60 to -19.55 and -19.55 to -14.81. We binned the galaxies in a way that there are always the same number of optical galaxies in each bin. We also confirm the trend found by Ledlow and Owen [1996] in which the fraction of galaxies in radio increases by raising the optical luminosity. The number of detections is higher in the first bin (optically bright galaxies) compared to the other two bins.

In Figure 3.4 we plotted the cumulative BRLF for A2256 (in black), and compared it to the BRLF from Ledlow and Owen [1996] (in green). To make a meaningful comparison, we used the same three bins of optical magnitudes as Ledlow and Owen [1996], high (-23.40 to -22.70), medium (-22.7 to -22.0) and low(-22.0 to -21.23).

There is a misleading discrepancy between the BRLF in figure 3.4 and the URLF we plotted in Figure 3.2. The URLF increases to values of 35% while the BRLF has a maximum value of 79% and 89% for the low and the middle bins, respectively (we ignored the high bin since there is only one source). The excess of the BRLF for A2256 partially comes from the fact that we only used the 16 brightest galaxies within the magnitude range of $-23.40 \geq M_r \leq -22.0$, and did not include faint galaxies. Most of the galaxies in the A2256 are faint and have absolute magnitudes greater than -22.0. Consequently, we have detected almost all of the optically bright galaxies in radio. Note that the Ledlow and Owen results are still biased because they normalized by only the elliptical galaxies and missing faint galaxies.

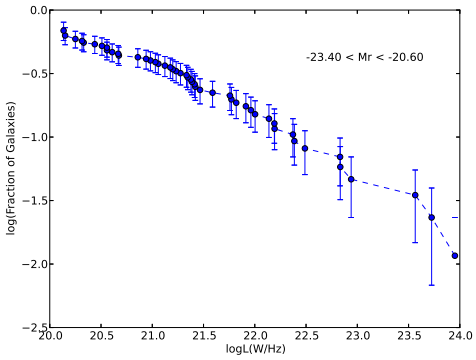

(a) $-23.40 < M_r < -20.60$

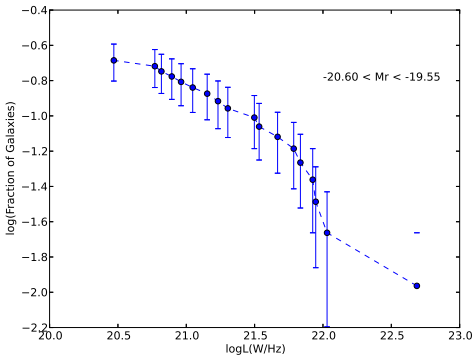

(b) $-20.60 < M_r < -19.55$

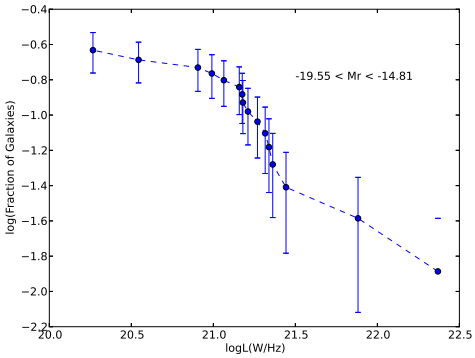

(c) $-19.55 < M_r < -14.81$

Figure 3.3 The cumulative BRLF for A2256 in three different bins of optical magnitude, (-23.40 to -20.60), (-20.60 to -19.55) and (-19.55 to -14.81).

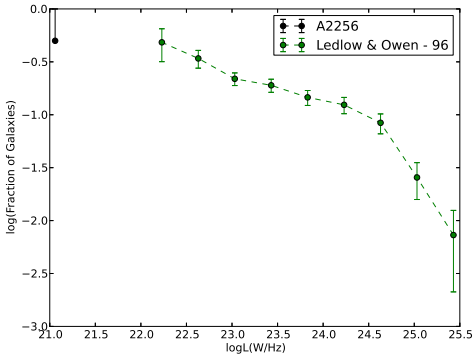

(a) $-23.40 < M_r < -22.70$

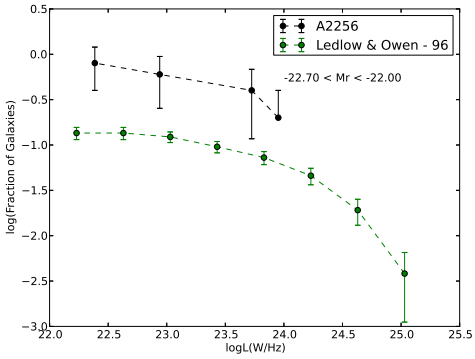

(b) $-22.70 < M_r < -22.00$

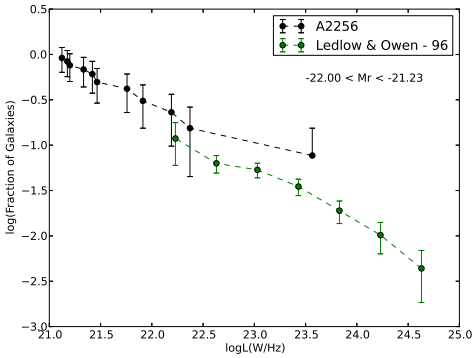

(c) $-22.00 < M_r < -21.23$

Figure 3.4 The cumulative BRLF for A2256 in three different bins of optical r band absolute magnitudes, high(-23.40 to -22.70), medium (-22.7 to -22.0) and low(-22.0 to -21.23). The black line shows the BRLF for A2256, and the green line is for the sample of galaxies from Ledlow and Owen [1996].

Chapter 4

Classification of galaxies

It is very common for galaxies with the most powerful radio emissions to be AGNs. As radio luminosity decreases star forming galaxies become dominant (Condon et al. [2002]; Mauch and Sadler [2007]).

Miller et al. [2009], in their Figure 9, plotted the RLF for the Coma cluster as well as the RLF for only AGNs and only Star Forming (SF) galaxies separately. They claimed that at the faint end of the RLF, AGNs become dominant. This is in contradiction with what most previous studies argued.

We can potentially investigate this issue for A2256, and calculate the RLF for only AGNs and Star Forming galaxies in the cluster. One of the best and most accurate methods for classifying galaxies as AGNs or SF is to use the galaxies' spectra and plot the famous Baldwin-Phillips-Terlevich (BPT) diagram (Kewley et al. [2001]). We tried to recover the spectra for our galaxies from the data in Berrington et al. [2002] (kindly provided by Berrington) since they reported spectroscopic redshifts for most of the cluster member galaxies. However, only a few of the spectra had high enough signal to noise to measure emission line fluxes and calculate the line ratios needed for the BPT diagram. Unfortunately, none of our radio sources were included in these spectra. We decided instead to classify our galaxies into two morphological groups, elliptical and spirals. It is known that AGNs are usually associated with the elliptical galaxies while most star forming activities happen in the spiral galaxies.

We classified our galaxies into ellipticals and spirals using the SDSS parameter fracDev which we described in Chapter 2. Masters et al. [2010] suggested that galaxies

with low fracDev can be safely identified as spiral galaxies. They proposed that the best possible fracDev classification cutoff is 0.6. According to Masters et al. [2010] galaxies with $fracDev < 0.6$ that are classified as spirals might have up to 10% contamination of elliptical galaxies, and objects with $fracDev > 0.6$ that are classified as elliptical galaxies could include 40% contamination of spiral galaxies. As a result, fracDev is a good parameter for identifying spiral galaxies. However, using it to find elliptical galaxies may not be the best approach.

Using fracDev=0.6 we found 52% of A2256's radio galaxies are in the elliptical class and 48% are in the spiral class. If we consider all the optical members of the cluster the fraction of spiral galaxies decreases to 33% while the remaining 67% are considered to be ellipticals. As mentioned before, there is always a probability of misclassification in each category. For example, the galaxy with the SDSS ID of 1237663230678794280 has a clear radio jet coming out from the nucleus but its fracDev is 0 which puts it into the spiral category. Radio objects with jets are very more likely to be associated with ellipticals. Another example of misclassification is the SDSS ID 1237663230678794604 which is more likely to be a SF galaxy based on the shape of the optical and radio images. One can see its spiral arms in the optical image and radio emission that extends beyond the area of optical emission in our radio map. Despite all this, the SDSS parameter fracDev is 1 which classifies this object as an elliptical galaxy. We visually inspected all galaxies, and changed the classification for these obviously misclassified objects as best we could.

Using our galaxy classification we plotted the URLF separately for spirals and ellipticals. Figure 4.1 shows the URLF for each class. The blue line is the URLF for spirals and the red line represents the elliptical galaxies. Spirals galaxies are mostly concentrated within the luminosity range of $10^{20.3}$ W/Hz to $10^{22.4}$ W/Hz while elliptical dominate the low and high end of the luminosity function,$L < 10^{20.3}$ W/Hz and $L > 10^{22.4}$ W/Hz.

There is an excess of spiral galaxies for most regions of the URLF. Even if we consider 10% contamination of ellipticals, the result is overwhelmingly likely to be the same. There is a deficit of elliptical galaxies for most regions of URLF. However, the high probability of contamination (40%) means that this is likely a significant overestimate of the number of ellipticals. As a result there is a possibility that the actual fractional

number of spirals is even larger than that measured.

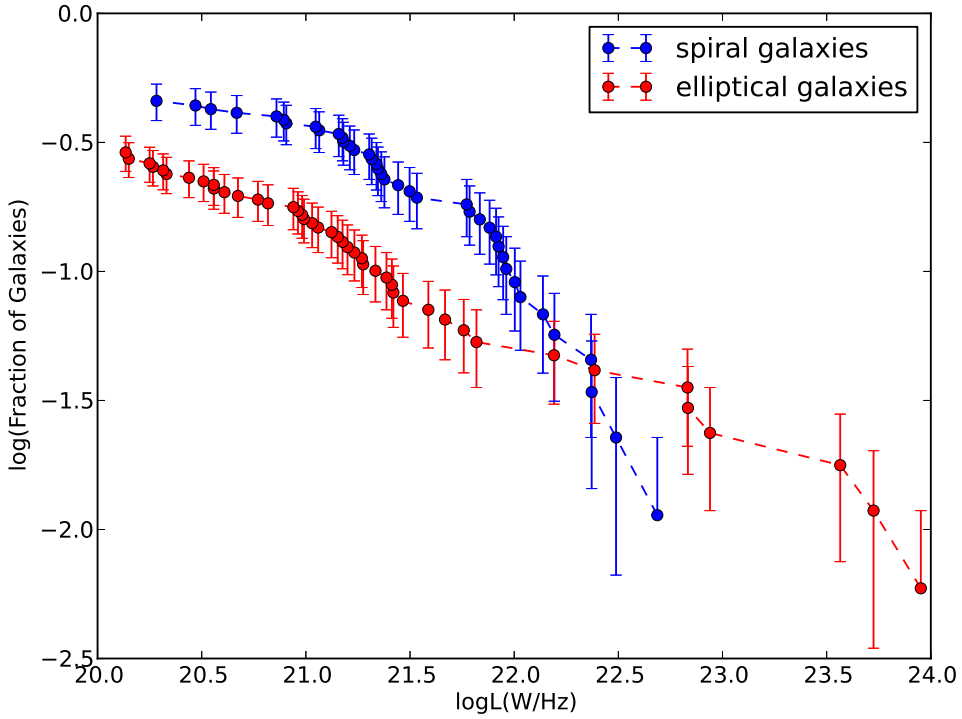

Figure 4.1 Univariate RLF for Spiral (blue) and Elliptical (red) galaxies in A2256. We classify galaxies as spirals and ellipticals using the SDSS parameter fracDev. Galaxies with $fracDev < 0.6$ are identified as spirals and those with $fracDev > 0.6$ as elliptical galaxies

Chapter 5

Galaxies in Abell 2256

5.1 Galaxy Distribution

In Figure 5.1 we plot the number of observable optical sources which is the number of optical galaxies in the sensitive area for radio object vs its radio luminosity, shown as the solid green line. Blue and red dots represent the number of enclosed optical sources, defined as the number of optical galaxies within the enclosed area (see Chapter 2) of each galaxy in the image. Blue dots represent spiral galaxies and red dots are elliptical galaxies, identified based on the value of parameter fracDev discussed in the last chapter.

For randomly distributed galaxies in the cluster we expect half of the radio galaxies to be above the dashed green line (half of the solid green line) and half of them below. However, Figure 5.1 shows that there are more galaxies above the dashed green line, meaning that there is a higher fraction of radio galaxies (60%) located far from the center than near the center (40%), relative to the optical distribution. If we exclude the brightest radio sources, then the distribution of radio galaxies below $10^{22.8}$ W/Hz is further biased to the outer optical galaxies, with fractions of 64(36)% above(below) the line.

Figure 5.1 also shows that there is a small population of faint sources in the radio that are located at the center of the cluster and are separated from other objects in this diagram. These faint sources show no obvious differences (such as optical magnitude, morphology and redshift) from the other galaxies.

This figure also shows that all very luminous sources in the radio are located at the center of the cluster. If we make a cut at a luminosity of $10^{22.8}$ we see that galaxies having a luminosity higher than this value are all located towards the center of the cluster.

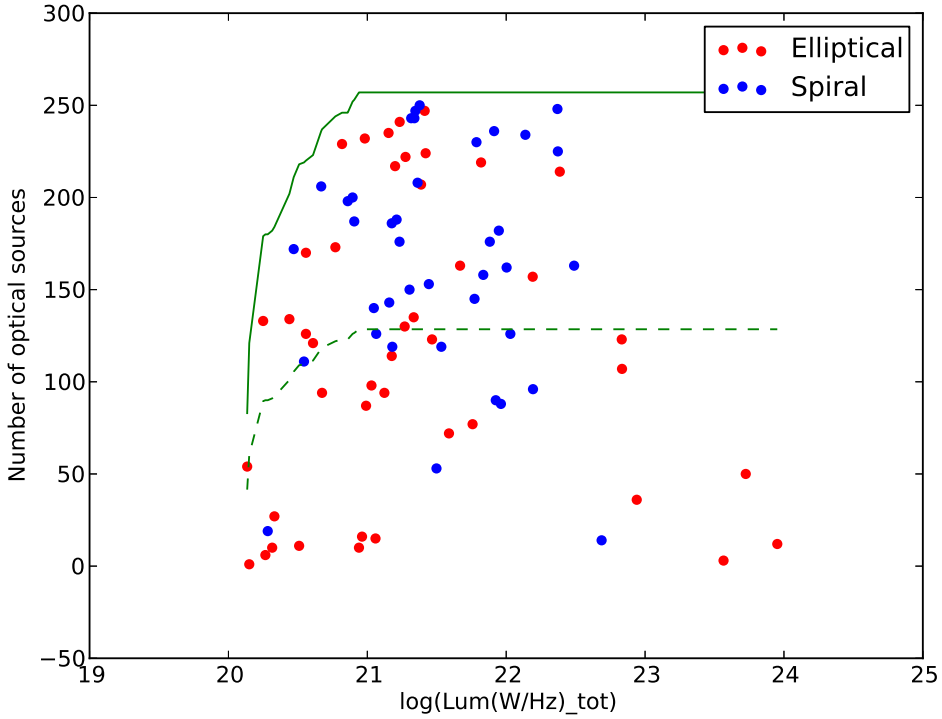

Figure 5.1 Number of cluster galaxies in the "enclosed area" vs Luminosity of radio galaxies. The solid green line is the number of cluster galaxies that could have been detected, which is all of the optical galaxies in the sensitive area for each radio source given its luminosity. The dashed green line is at half the value of the solid green line. The red dots are for elliptical galaxies and the blue dots are for spirals based on their fracDev value.

5.2 Radio Galaxy Structure

The radio emission from galaxies is synchrotron emission that is created as a result of relativistic electrons formed by AGNs or supernova remnant shocks in star forming

galaxies. Morphologically, there are three kinds of radio sources compact, extended and jet/lobe.

Spiral galaxies which are more likely to have star forming activities are extended over the same area in the radio as in the optical. For example, in Figure 2.2 (a), the spiral arms that are sites of ongoing star formation also emit in radio. If we observe a galaxy that is a large spiral or disk galaxy and has emission extending over the galaxy face then it almost certainly SF. If we observed the compact emission it's either the emission, from AGN or SF activities from the center of galaxy and if we observed a jet or other very extended emission it's definitely AGN. The classification of galaxies as compact(comp), extended(ext) and jet, is given in table 2. We also include the classification of Miller et al. [2003b] for some galaxies in A2256. If the galaxy is already classified by Miller et al. [2003b] we label them as AGN or SF.

In Figure 5.1 red dots represent the elliptical galaxies and blue dots are spirals, using the fracDev parameter as we explained earlier. We can see that most galaxies that are close to the center are elliptical galaxies. All very high radio luminosity sources are elliptical galaxies. Most of the very low radio luminosity galaxies are elliptical galaxies as well, although there is an expected 40% spiral contamination rate using fracDev. Also most of spiral galaxies are distributed far from the center of the cluster.

Chapter 6

Discussion

We now present the summary of our results followed by a discussion of interesting findings:

i) We identified 275 cluster members for A2256 of which 83 are radio sources with $log(luminosity) > 20.135$ W/Hz. The detections are complete above the luminosity of $log(luminosity) > 20.94$ W/Hz. Two additional possible radio identifications are not included.

ii) Most of the radio sources in A2256 have low luminosity, $log(Lum) < 22.8$ W/Hz. Comparing the A2256 RLF to a sample of clusters of galaxies from Ledlow and Owen [1996], we detected more faint sources but fewer of the very brightest ones in the radio. However, if we only look at the galaxies with optical magnitudes in the same range as Ledlow and Owen [1996], we detected a greater fraction of galaxies.

iii) The RLF of A2256 is almost the same as that of the Coma cluster.

iv) Most of the radio sources in A2256 are proportionately located further from the center than the optical galaxies. Also, there is a possibility that the density of radio sources is lower at the position of the radio relic.

v) Most of the very luminous radio sources that are associated with elliptical galaxies are located close to the core of the cluster, and most spiral radio galaxies are located farther from the core of the cluster.

vi) There is a group of very faint sources that are at the center of the cluster. Eight out of nine are associated with galaxies classified as elliptical, using the fracDev values from SDSS.

vii) Only 33% of all cluster members are spiral galaxies and the rest are ellipticals, using fracDev. Moreover, 47% of radio galaxies are spirals and 53% are ellipticals. However, it should be noted that up to 40% of galaxies classified as ellipticals may actually be spirals. This means that a much higher proportion of cluster spiral galaxies show radio emission than the proportion of ellipticals.

We are trying to answer the following questions in this paper. How does cluster-cluster merging affect the evolution of individual galaxies in the cluster? Do these kinds of merging trigger more radio activity in the galaxies in the cluster? Are the SF activities quenched or enhanced due to mergers? Are AGNs going to increase or decrease due to cluster merging?

Bekki [1999] simulated the merging process of a small group of galaxies with a cluster and followed the dynamic evolution of a gas-rich late-type spiral galaxy during this process. The time-dependent tidal gravitational field from the merging activity perturbs the galaxy disk and makes a stellar bar at the center and gaseous spiral arms in the galaxy. The increased collisions between clouds due to the new structure and the dissipation of gas, transfer the gas to the central region of the galaxy and, as a result, induce starburst activity.

In addition, according to Miller and Owen [2003] the consistency between AGN and X-ray emission from galaxies shows AGN activity increases due to cluster merging.

There are several studies (for example Miller et al. [2009], Owen et al. [2005]) on Abell clusters, trying to answer the questions stated previously. Owen et al. [1999] found that, although A2125 and A2645 are at the same redshift and have same richness class as each other, A2645 is more virialized with less blue galaxies and A2125 is undergoing cluster-cluster merging and consists of more blue galaxies. There are more detections of radio galaxies for A2125 compared to A2156. This leads to the conclusion that cluster merging can be responsible for these activities. Miller and Owen [2003] also suggested that the cluster-cluster merging is responsible for the enhancement of SF and AGNs in A2255.

Abell 2256 is one of the rich clusters with an ongoing cluster-cluster merger. Therefore, it is a good candidate to examine the hypothesis about the evolution of each galaxy in the merging cluster. High resolution and deep radio images from VLA help us to see more details and detect more radio galaxies in the cluster and, as a result we have

better statistics for our results.

We now discuss our results from our RLF analysis comparison of A2256 and Coma. Both clusters have similar RLF (with A2256 having a small excess in its RLF). This may be explained by the following similarities. Both clusters have a richness class of 2; both are undergoing cluster-cluster merging; and both are known to be dynamically evolved clusters. Coma and A2256 are both late Bautz-Morgan type (Bautz and Morgan [1970]), rich and centrally condensed with high velocity dispersions, high X-ray temperatures, high X-ray luminosities, and X-ray core radii of ~ 0.5 Mpc.

From the results in Figure 5.1, we can see that most radio galaxies in A2256 are faint and located on the outer part of the cluster except the group of very faint radio sources that are located near the center of the cluster. On the other hand, as you can see in Figure 1.1, the density of sources that are located to the west of the relic is greater than the density of those in the relic. This may be due to the difficulty of identifying individual radio sources due to confusion from the filamentary structure of the relic.

Figure 4.1 plots the URLF separately for both spiral and elliptical galaxies. At high luminosities a large fraction of the galaxies are elliptical, and for lower luminosities spiral galaxies dominate. The BRLF can give additional information beyond the URLF since it also uses optical magnitude. From the cumulative BRLF for A2256 we can see that the probability for a galaxy to have a radio counterpart increases as the optical luminosity goes up. Ledlow and Owen [1996] obtained the same result and showed that (figure 8 in Ledlow and Owen [1996]) galaxies brighter than an absolute magnitude of -22.4 are about 2.5 times more likely to have radio emission.

To answer the posed questions more precisely, it would be very helpful to break the sample into SF and AGN to see the effect of merging in more detail for each galaxy type. Unfortunately, due to the lack of spectra, we were not able to classify our galaxies as SF or AGN. However, knowing that AGNs are usually associated with elliptical galaxies and SF activities are much greater in spirals, we classified our galaxies as spiral or elliptical galaxies (Using SDSS parameter fracDev). It should be taken into account that fracDev doesn't give us the most accurate classification for elliptical galaxies since roughly 40% of these are expected to actually be spirals. However, it can classify spiral galaxies with only a 10% contamination by ellipticals.

We know from our analysis using fracDev that there are fewer optical spiral galaxies

than elliptical . However, the number of radio galaxies that are spiral roughly equals the number of elliptical radio galaxies. Especially when we account for the 40% contamination rate, the number of radio spirals is likely to exceed the number of radio ellipticals. As we mentioned, cluster merging can change the morphology of the galaxy from disk shape to barred shape galaxies (Bekki [1999]). Because of this, the enhancement of spirals in radio can be due to the cluster merging which triggers more SF activity.

FracDev offers additional information about the color of galaxies. Objects with higher values of fracDev always have redder face-on colors compare to those with smaller value of fracDev (Masters et al. [2010]). From the Butcher-Oemler effect, the fraction of blue galaxies in the core of cluster is low for clusters at lower redshift. We can see this effect in A2256, since A2256 is considered a low redshift cluster and as we can see from Figure 5.1, most of spiral galaxies are located at the outskirts of the cluster.

Does the ongoing cluster merging in A2256 trigger more SF and AGN activity? This important question has yet to be answered. Getting spectra for galaxies in the cluster and classifying them as SF or AGNs can be the first step to better understand changes due to merging in A2256. This will also allow us to determine the fractional occurrence of AGN and SF in elliptical and spiral galaxies in dynamically active clusters. This information may be useful for other studies which don't have spectra and therefore cannot classify AGN and SF.

Future work will also confirm or reject the important result of Miller et al. [2009] who argue that, in the Coma cluster, at values $log(Lum) < 21$ W/Hz, AGNs dominate over SF. However, their study suffers from the low number of galaxies detected as cluster members and therefore has a large uncertainty. Since our study of A2256 doesn't have this problem, we can test this result and see if the same phenomena happen in this cluster.

Last but not least, getting X-ray data with higher resolution can help us to understand the evolution of AGNs during the merger.

Chapter 7

Notes on individual radio galaxies

In this section we provide more explanation on some of the radio objects where there is a possible ambiguity with the optical identification. We show the corresponding optical images in Figure 7.1, where the cyan contours are radio emission, and the red cross shows the position of the galaxy we include in our sample.

a) 1237663269332058258: The optical position from NED is off from the nucleus of the galaxy. We changed the optical position to the correct one.

b) 1237663269868994575: There are two interacting optical sources but only the southern source is a radio object. According to NED, there is only one position and redshift assigned to these two sources. The position from NED is located somewhere between the two galaxies. We considered the southern radio source as a member of the cluster, and changed the optical position to the position of its optical nucleus.

c) 1237663269868929419: The center of the radio source associated with the galaxy does not match with the optical nucleus. However, given the optical structure in the south east, there is a possibility of interaction of this galaxy with another galaxy, so we include this in the radio sample.

d) 1237663269868994834: Optical and radio centers are not at the same position, and are separated by 2.4 arcsec; it is included in the radio sample.

e) 1237663269868994713 and 1237663269868994714: There are two radio sources, but only the eastern source (1237663269868994713) has a redshift in NED. Their envelopes are overlapping which could be a sign of an interacting system. We assumed both sources are at the same redshift, and are members of the cluster. Both of these

sources are included in our sample.

f) 1237663269868994760: There are three galaxies, but we only have the redshift of the southern-western one. Since the envelope of the optical galaxies are touching we included the nothern-eastern object that has a radio counterpart in our sample. It seems they all belong to one interacting system.

g) 1237656565428060410 : There are two radio sources which could be associated with each other. However there is only one optical counterpart. It should be noted that these radio sources are located in the vicinity of the radio relic, and their measured radio flux densities might be contaminated.

h) 1237656565428060275 , 1237656565428060276 and 1237656565428060273: This is the NGC6331 triple system. More detailed information about this system can be found in Owen et al. [2014]. There is another radio source to the North-east of this system; it has no available redshift, so we did not include the radio source in our sample.

i) 1237663230678794442: There is an additional radio source at the north-west of the optical galaxy with no measured redshift so we did not include it in our sample. However, it is possible that the north-west source also belong to the cluster.

j)1237663230678794725 : There is a additional radio source at the North-East of the optical galaxy with no redshift. We did not include it in our sample.

k)1237663269868994759 : There is a second radio source six arcsec away to the east side and very close to the jet of the large tailed radio source. They have a common envelope in their optical images, and therefore, they both might be cluster members However, we do not use it in our sample.

l) 1237663230678794786: Near this radio object, there are several extra radio sources with unknown redshift. We did not include them in our sample as cluster members.

m)1237663269868929212: This source is a cluster member but since the optical and radio centers did not match we did not include it in our radio sample.

n)1237663269332123887: This source is a cluster member but since the optical and radio centers did not match we did not include it in our radio sample.

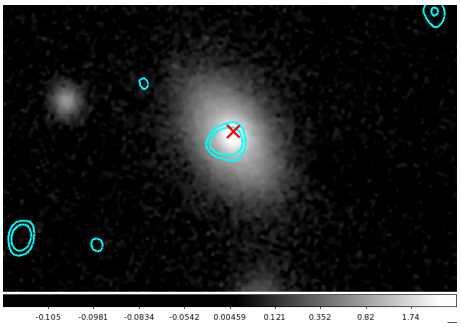
-0.105 -0.0981 -0.0834 -0.0542 0.00459 0.121 0.352 0.82 1.74

(a)

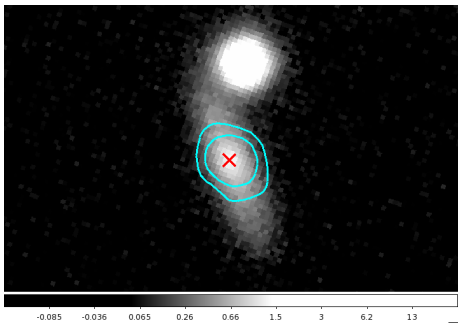
-0.085 -0.036 0.065 0.26 0.66 1.5 3 6.2 13

(b)

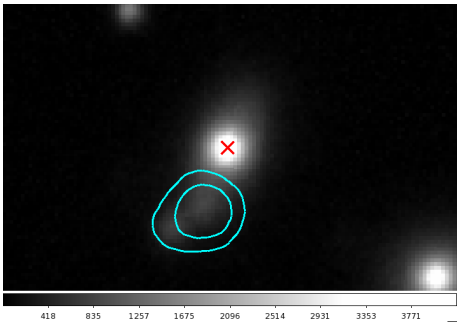
418 835 1257 1675 2096 2514 2931 3353 3771

(c)

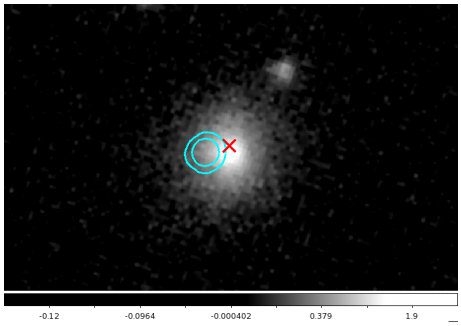
-0.12 -0.0964 -0.000402 0.379 1.9

(d)

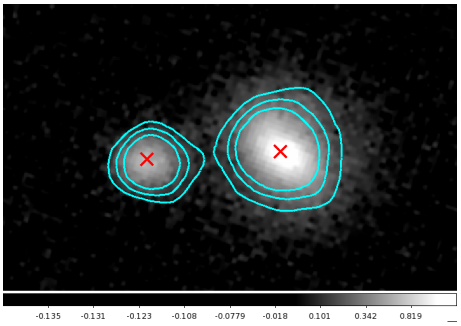
-0.135 -0.131 -0.123 -0.108 -0.0779 -0.018 0.101 0.342 0.819

(e)

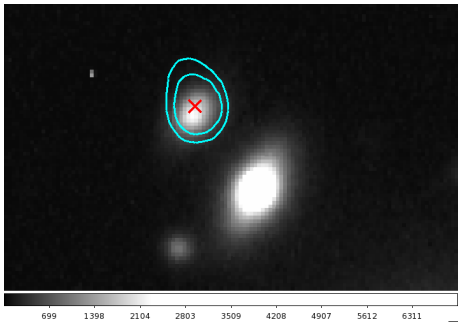
699 1398 2104 2803 3509 4208 4907 5612 6311

(f)

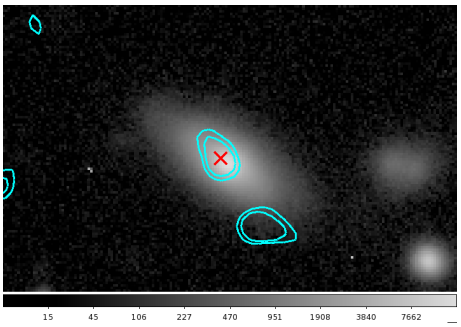
15 45 106 227 470 951 1908 3840 7662

(g)

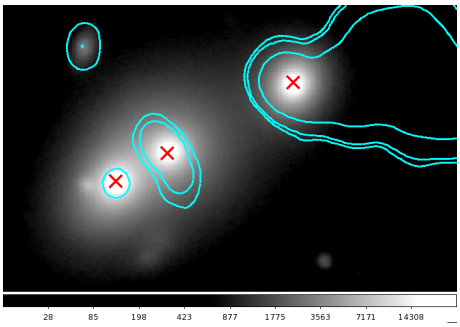
28 85 198 423 877 1775 3563 7171 14308

(h)

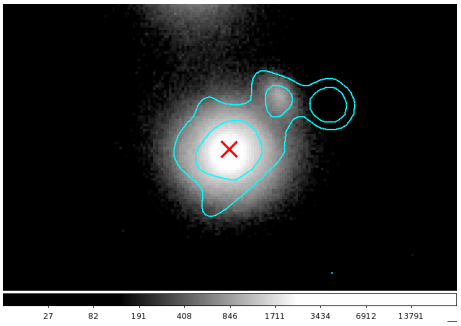
27 82 191 408 846 1711 3434 6912 13791

(i)

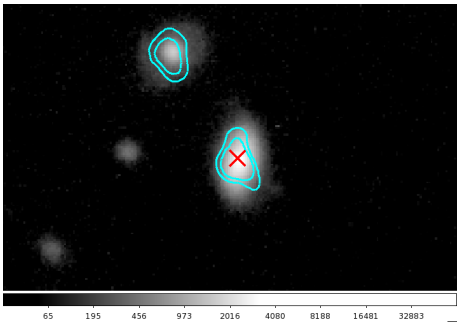
65 195 456 973 2016 4080 8188 16481 32883

(j)

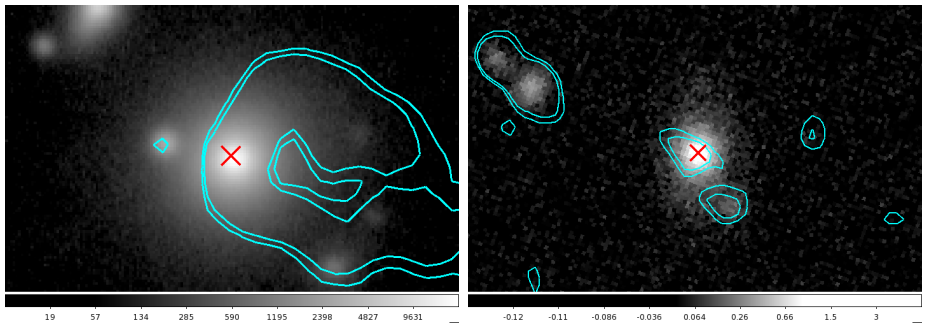

(k) (l)

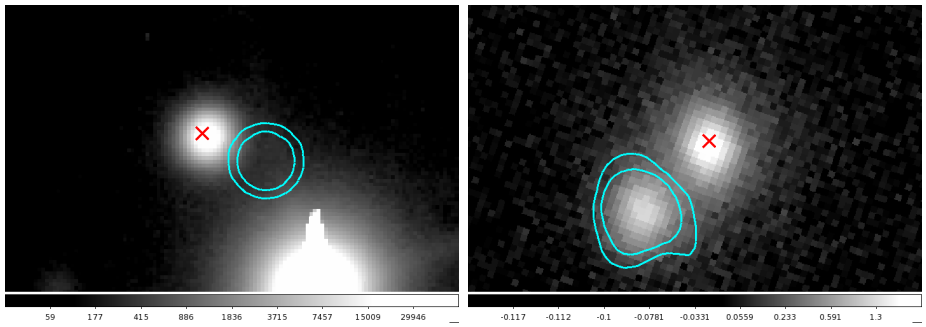

(m) (n)

Figure 7.1 Optical images of galaxies that have been mentioned in section 9. The cyan contours are radio contours. The red cross is the galaxy we used in our sample

References

L. P. Bautz and W. W. Morgan. On the Classification of the Forms of Clusters of Galaxies. *APJL*, 162:L149, December 1970. doi: 10.1086/180643.

K. Bekki. Group-Cluster Merging and the Formation of Starburst Galaxies. *APJl*, 510: L15–L19, January 1999. doi: 10.1086/311796.

R. C. Berrington, P. M. Lugger, and H. N. Cohn. The Dynamics of the Merging Galaxy Cluster System A2256: Evidence for a New Subcluster. *AJ*, 123:2261–2279, May 2002. doi: 10.1086/339840.

G. Brunetti and T. W. Jones. Cosmic Rays in Galaxy Clusters and Their Interaction with Magnetic Fields. In A. Lazarian, E. M. de Gouveia Dal Pino, and C. Melioli, editors, *Astrophysics and Space Science Library*, volume 407 of *Astrophysics and Space Science Library*, page 557, 2015. doi: 10.1007/978-3-662-44625-6-20.

T. E. Clarke and T. A. Ensslin. Deep 1.4 GHz Very Large Array Observations of the Radio Halo and Relic in Abell 2256. *AJ*, 131:2900–2912, June 2006. doi: 10.1086/504076.

J. J. Condon, W. D. Cotton, and J. J. Broderick. Radio Sources and Star Formation in the Local Universe. *AJ*, 124:675–689, August 2002. doi: 10.1086/341650.

A. Dressler. A catalog of morphological types in 55 rich clusters of galaxies. *APJS*, 42: 565–609, April 1980. doi: 10.1086/190663.

A. Dressler, I. Smail, B. M. Poggianti, H. Butcher, W. J. Couch, R. S. Ellis, and A. Oemler, Jr. A Spectroscopic Catalog of 10 Distant Rich Clusters of Galaxies. *APJS*, 122:51–80, May 1999. doi: 10.1086/313213.

C. Ferrari. Star Formation in Merging Galaxy Clusters. In S. Röser, editor, *Reviews in Modern Astronomy*, volume 18 of *Reviews in Modern Astronomy*, pages 147–163, September 2005. doi: 10.1002/3527608966.ch7.

Y. Fujita. Quantitative Estimates of Environmental Effects on the Star Formation Rate of Disk Galaxies in Clusters of Galaxies. *APJ*, 509:587–594, December 1998. doi: 10.1086/306518.

Y. Fujita, M. Takizawa, M. Nagashima, and M. Enoki. Is Galactic Star-Formation Activity Increased during Cluster Mergers? *PASJ*, 51:L1–L5, June 1999. doi: 10.1093/pasj/51.3.L1.

R. Gilmour, M. E. Gray, O. Almaini, P. Best, C. Wolf, K. Meisenheimer, C. Papovich, and E. Bell. Environmental dependence of active galactic nuclei activity in the supercluster A901/2. *MNRAS*, 380:1467–1487, October 2007. doi: 10.1111/j.1365-2966.2007.12127.x.

D. Haggard, P. J. Green, S. F. Anderson, A. Constantin, T. L. Aldcroft, D.-W. Kim, and W. A. Barkhouse. The Field X-ray AGN Fraction to z = 0.7 from the Chandra Multiwavelength Project and the Sloan Digital Sky Survey. *APJ*, 723:1447–1468, November 2010. doi: 10.1088/0004-637X/723/2/1447.

L. J. Kewley, M. A. Dopita, R. S. Sutherland, C. A. Heisler, and J. Trevena. Theoretical Modeling of Starburst Galaxies. *APJ*, 556:121–140, July 2001. doi: 10.1086/321545.

M. J. Ledlow and F. N. Owen. 20 CM VLA Survey of Abell Clusters of Galaxies. VI. Radio/Optical Luminosity Functions. *AJ*, 112:9, July 1996. doi: 10.1086/117985.

K. L. Masters, R. Nichol, S. Bamford, M. Mosleh, C. J. Lintott, D. Andreescu, E. M. Edmondson, W. C. Keel, P. Murray, M. J. Raddick, K. Schawinski, A. Slosar, A. S. Szalay, D. Thomas, and J. Vandenberg. Galaxy Zoo: dust in spiral galaxies. *MNRAS*, 404:792–810, May 2010. doi: 10.1111/j.1365-2966.2010.16335.x.

T. Mauch and E. M. Sadler. VizieR Online Data Catalog: Radio sources in the 6dFGS (Mauch+, 2007). *VizieR Online Data Catalog*, 837:50931, September 2007.

C. J. Miller, R. C. Nichol, P. L. Gómez, A. M. Hopkins, and M. Bernardi. The Environment of Active Galactic Nuclei in the Sloan Digital Sky Survey. *APJ*, 597:142–156, November 2003a. doi: 10.1086/378383.

N. A. Miller and F. N. Owen. Abell 2255: Increased Star Formation and AGN Activity in a Cluster-Cluster Merger. *AJ*, 125:2427–2446, May 2003. doi: 10.1086/374767.

N. A. Miller, F. N. Owen, and J. M. Hill. A Comprehensive Radio and Optical Study of Abell 2256: Activity from an Infalling Group. *AJ*, 125:2393–2410, May 2003b. doi: 10.1086/374628.

N. A. Miller, A. E. Hornschemeier, B. Mobasher, T. J. Bridges, M. J. Hudson, R. O. Marzke, and R. J. Smith. The Radio Luminosity Function and Galaxy Evolution in the Coma Cluster. *AJ*, 137:4450–4467, May 2009. doi: 10.1088/0004-6256/137/5/4450.

B. Mobasher, M. Colless, D. Carter, B. M. Poggianti, T. J. Bridges, K. Kranz, Y. Komiyama, N. Kashikawa, M. Yagi, and S. Okamura. A Photometric and Spectroscopic Study of Dwarf and Giant Galaxies in the Coma Cluster. IV. The Luminosity Function. *APJ*, 587:605–618, April 2003. doi: 10.1086/368305.

F. N. Owen, M. J. Ledlow, W. C. Keel, and G. E. Morrison. Cluster Mergers as Triggers of Star Formation and Radio Emission: A Comparative Study of the Rich Clusters Abell 2125 and 2645. *AJ*, 118:633–644, August 1999. doi: 10.1086/300974.

F. N. Owen, W. C. Keel, M. J. Ledlow, G. E. Morrison, and R. A. Windhorst. A Deep Radio Survey of Abell 2125. I. Radio, Optical, and Near-Infrared Observations. *AJ*, 129:26–30, January 2005. doi: 10.1086/426322.

F. N. Owen, L. Rudnick, J. Eilek, U. Rau, S. Bhatnagar, and L. Kogan. Wideband Very Large Array Observations of A2256. I. Continuum, Rotation Measure, and Spectral Imaging. *APJ*, 794:24, October 2014. doi: 10.1088/0004-637X/794/1/24.

K. A. Pimbblet, S. S. Shabala, C. P. Haines, A. Fraser-McKelvie, and D. J. E. Floyd. The drivers of AGN activity in galaxy clusters: AGN fraction as a function of mass and environment. *MNRAS*, 429:1827–1839, February 2013. doi: 10.1093/mnras/sts470.

M. Sun, S. S. Murray, M. Markevitch, and A. Vikhlinin. Chandra Observation of A2256: A Cluster at the Early Stage of Merging. *APJ*, 565:867–876, February 2002. doi: 10.1086/324721.

R. J. van Weeren, H. T. Intema, J. B. R. Oonk, H. J. A. Röttgering, and T. E. Clarke. The discovery of diffuse steep spectrum sources in Abell 2256. *AAP*, 508:1269–1273, December 2009. doi: 10.1051/0004-6361/200912934.

H. K. C. Yee, E. Ellingson, and R. G. Carlberg. The CNOC Cluster Redshift Survey Catalogs. I. Observational Strategy and Data Reduction Techniques. *APJS*, 102:269, February 1996. doi: 10.1086/192259.

Appendix A

Tables

Table A.1: **Optical information for radio galaxy members**

SDSS ID	**RA (degree)**	**DEC (degree)**	**Redshift**	**Mag$_r$**	**fracDev$_r$**
1237656565428060275	255.90000	78.62890	0.054	13.73	0.78
1237656565428060276	255.89210	78.63000	0.056	16.69	0.00
1237656565428060273	255.87290	78.63190	0.059	14.92	1.00
1237656565428060594	255.76210	78.59890	0.055	14.91	1.00
1237656565428060462	255.87540	78.66530	0.059	15.14	1.00
1237656565427995029	255.21750	78.68920	0.058	15.58	0.97
1237663230678794604	256.41290	78.62560	0.054	15.32	1.00
1237663269868994759	256.73460	78.68580	0.056	15.51	1.00
1237663230678794280	256.68040	78.59920	0.050	17.14	0.00
1237663269868929406	255.98580	78.74560	0.057	15.65	0.83
1237656565428060249	255.56290	78.59640	0.062	15.50	1.00
1237656565427994941	255.84290	78.78220	0.065	16.54	0.04
1237663269868929086	256.20040	78.64140	0.063	14.77	1.00
1237656565427995051	255.34710	78.68750	0.054	15.77	0.00
1237655749380800844	254.57670	78.49280	0.060	15.07	0.10
1237655749380866230	254.69500	78.42280	0.052	15.21	0.38
1237656565428060200	255.79960	78.67500	0.052	15.86	0.92
1237663269868929392	256.06830	78.67920	0.052	15.69	0.96
1237656565428060284	256.11330	78.64030	0.059	13.41	0.48

Continued on next page

Table A.1 – *Continued from previous page*

SDSS ID	RA (degree)	DEC (degree)	Redshift	Mag_r	$fracDev_r$
1237656565428060521	255.70540	78.64140	0.056	16.19	0.95
1237663269868929591	256.23750	78.71830	0.062	17.37	0.01
1237656565427994915	255.57420	78.76440	0.066	16.28	0.61
1237663230678728929	256.39130	78.58670	0.063	15.20	0.84
1237656565427994914	255.57710	78.76780	0.065	15.95	0.36
1237656565428060547	255.37380	78.60190	0.060	15.94	1.00
1237663269868929533	256.20290	78.80580	0.066	15.27	1.00
1237663269868994713	256.30000	78.80390	0.066	16.59	0.41
1237663269868994714	256.31370	78.80370	0.066	18.28	0.00
1237656565427995060	255.13420	78.67000	0.060	15.58	1.00
1237656565427994887	255.24630	78.74970	0.053	15.37	0.97
1237656565427994707	255.24960	78.75890	0.057	17.59	0.37
1237656565428060420	255.12210	78.63470	0.059	16.12	1.00
1237663230678794582	256.54920	78.54720	0.061	15.11	1.00
1237663269868994575	256.24370	78.83300	0.065	16.80	0.13
1237656565428125957	255.97380	78.48670	0.054	17.59	0.12
1237663231215599976	255.89380	78.84860	0.063	16.28	0.00
1237663230678794442	256.86250	78.60580	0.059	16.38	0.22
1237663269868994718	256.23130	78.85220	0.067	17.44	0.07
1237656565427929453	255.69500	78.86280	0.055	15.35	1.00
1237663269868994787	256.61830	78.82080	0.063	17.28	0.18
1237656565427929429	255.55130	78.85920	0.064	16.10	0.13
1237656565427929436	255.39290	78.84610	0.065	16.79	0.63
1237663269868994741	256.39000	78.85470	0.066	16.01	0.28
1237663230678794779	257.04540	78.65330	0.050	17.36	0.14
1237656565427929475	255.08130	78.81030	0.051	15.80	0.89
1237656565427929441	255.10630	78.82420	0.051	16.85	0.00
1237663230678794662	256.81580	78.50220	0.063	16.92	0.00
1237663231215665398	256.06040	78.91000	0.063	18.14	0.34
1237663230678794725	257.01330	78.54420	0.060	17.61	0.00
1237656565427929379	255.57040	78.90310	0.065	17.88	0.40
1237655749380800875	254.90630	78.49530	0.053	16.12	0.32

Continued on next page

Table A.1 – *Continued from previous page*

SDSS ID	**RA** (degree)	**DEC** (degree)	**Redshift**	**Mag**$_r$	**fracDev**$_r$
1237655749380735063	254.58670	78.72390	0.053	16.90	0.33
1237663269332058258	256.63960	78.42190	0.060	15.71	0.47
1237663269332058626	256.54790	78.41060	0.061	17.52	0.00
1237663230678794417	257.13960	78.49830	0.062	14.92	1.00
1237663269869060123	257.24210	78.83750	0.054	15.43	0.99
1237656565427929306	255.13460	78.93610	0.051	16.11	0.65
1237663230678794786	257.32790	78.50470	0.056	16.91	0.82
1237656565428191416	255.85330	78.34420	0.063	16.70	0.00
1237663230678859802	257.43000	78.51780	0.062	16.35	0.87
1237656565428060410	255.78880	78.68890	0.048	16.37	1.00
1237663231215665231	256.15630	78.88890	0.060	17.55	0.46
1237663231215599942	255.45500	79.03780	0.064	19.06	0.00
1237663269868994834	256.97960	78.74690	0.057	16.45	0.77
1237663230678860038	257.41460	78.55220	0.054	15.37	0.76
1237663230678794278	256.70420	78.59280	0.058	16.24	1.00
1237663269868994760	256.75210	78.68970	0.057	17.52	0.86
1237655749380800577	254.50500	78.56280	0.064	15.18	1.00
1237656565427995115	255.33420	78.75560	0.057	18.21	0.14
1237656565427863896	255.04460	79.00440	0.058	16.28	0.99
1237656565427864068	254.95420	78.97220	0.059	18.12	0.00
1237663269869060336	257.29130	78.87560	0.063	15.54	0.04
1237663269868929419	256.14960	78.66810	0.066	17.18	0.73
1237663269868929423	255.90920	78.78280	0.066	17.53	0.92
1237655749380669721	254.19670	78.78310	0.057	15.95	0.80
1237655749380800829	254.71420	78.51670	0.062	15.99	0.85
1237663269332189441	257.63000	78.48610	0.053	16.35	0.33
1237663269332123864	257.19830	78.43220	0.056	16.70	0.65
1237663269332123998	257.17420	78.39580	0.057	17.52	0.15
1237655749380931763	255.53040	78.29170	0.059	15.53	0.40
1237663230678794711	256.78250	78.64280	0.063	15.64	0.99
1237656565428060463	255.89880	78.66500	0.052	16.34	0.96
1237656565428061022	255.95200	78.64570	0.057	19.97	1.00

Continued on next page

Table A.1 – *Continued from previous page*

SDSS ID	**RA (degree)**	**DEC (degree)**	**Redshift**	**Mag$_r$**	**fracDev$_r$**
1237663269868929212	256.28580	78.68500	0.059	16.66	0.00
1237663269332123887	257.34130	78.36830	0.054	16.68	1.00

Table A.2: **Radio information for radio galaxy members**

SDSS ID	**RA** (degree)	**DEC** (degree)	**Area**$_{enc}$ (Mpc^2)	**Area**$_{obs}$ (Mpc^2)	**flux** (μ**Jy**)	**flux**$_p$ (μ**Jy**)	**log(lum)** (**W/Hz**)	**N**$_{enc}$	**N**$_{obs}$	**radio morphology**
1237656565428060275	255.89829	78.62892	0.09	10.25	155	68	21.059	15	257	comp
1237656565428060276	255.89138	78.62978	0.08	10.25	6585	296	22.687	14	257	ext
1237656565428060273	255.87238	78.63203	0.08	10.25	121250	22135	23.952	12	257	AGN
1237656565428060594	255.76154	78.59875	0.34	10.25	71953	1659	23.725	50	257	AGN
1237656565428060462	255.87517	78.66517	0.01	10.25	49700	2821	23.565	3	257	AGN
1237656565427995029	255.21750	78.68928	1.19	10.25	9253	1790	22.834	107	257	AGN
1237663230678794604	256.41479	78.62625	0.63	10.25	775	50	21.758	77	257	ext(SF)
1237663269868994759	256.73421	78.68597	1.49	10.25	9190	365	22.832	123	257	Jet
1237663230678794280	256.68008	78.59925	1.55	10.25	1451	846	22.030	126	257	Jet
1237663269868929406	255.98562	78.74553	0.37	0.76	18	18	20.135	54	83	AGN
1237656565428060249	255.56242	78.59647	0.60	10.25	524	150	21.588	72	257	ext
1237656565427994941	255.84267	78.78222	0.81	10.25	1140	213	21.925	90	257	ext
1237663269868929086	256.20029	78.64156	0.20	10.25	11792	4240	22.940	36	257	AGN
1237656565427995051	255.34846	78.68753	0.80	10.25	1241	150	21.962	88	257	ext
1237655749380800844	254.57683	78.49278	6.03	10.25	3189	272	22.372	225	257	ext(SF)
1237655749380866230	254.69696	78.42261	7.06	10.25	1109	98	21.913	236	257	AGN
1237656565428060200	255.79850	78.67494	0.04	3.40	28	23	20.315	10	182	ext
1237663269868929392	256.06771	78.67922	0.05	10.25	118	111	20.940	10	257	comp
1237656565428060284	256.11221	78.64036	0.12	3.27	26	23	20.283	19	180	comp
1237656565428060521	255.70408	78.64133	0.16	3.47	29	34	20.331	27	184	comp
1237663269868929591	256.23592	78.71828	0.37	10.25	426	127	21.498	53	257	ext
1237656565427994915	255.57375	78.76450	0.86	7.10	64	52	20.674	94	237	ext

Continued on next page

Table A.2 – *Continued from previous page*

SDSS ID	**RA** (degree)	**DEC** (degree)	**Area**$_{enc}$ (Mpc^2)	**Area**$_{obs}$ (Mpc^2)	**flux** (μ**Jy**)	**flux**$_p$ (μ**Jy**)	**log(lum)** (**W/Hz**)	**N**$_{enc}$	**N**$_{obs}$	**radio morphology**
1237663230678728929	256.39054	78.58661	0.86	10.25	180	160	21.123	94	257	comp
1237656565427994914	255.57625	78.76778	0.89	10.25	2113	457	22.193	96	257	SF
1237656565428060547	255.37346	78.60208	0.96	10.25	145	140	21.030	98	257	comp
1237663269868929533	256.20229	78.80589	1.31	10.25	203	175	21.176	114	257	comp
1237663269868994713	256.30017	78.80397	1.42	10.25	462	201	21.533	119	257	SF
1237663269868994714	256.31367	78.80369	1.44	10.25	205	127	21.180	119	257	comp
1237656565427995060	255.13358	78.67000	1.45	5.78	55	59	20.609	121	223	comp
1237656565427994887	255.24613	78.74983	1.47	10.25	396	400	21.466	123	257	AGN
1237656565427994707	255.25008	78.75856	1.55	10.25	157	84	21.064	126	257	ext
1237656565428060420	255.12392	78.63511	1.55	5.61	49	29	20.558	126	220	ext
1237663230678794582	256.54846	78.54711	1.72	10.25	292	277	21.334	135	257	comp
1237663269868994575	256.24379	78.83314	1.86	10.25	151	115	21.047	140	257	comp
1237656565428125957	255.97329	78.48656	1.92	10.25	195	159	21.158	143	257	ext
1237663231215599976	255.89346	78.84858	1.96	10.25	801	190	21.772	145	257	SF
1237663230678794442	256.86104	78.60622	2.20	10.25	273	56	21.304	150	257	ext
1237663269868994718	256.22996	78.85225	2.23	10.25	376	206	21.443	153	257	comp
1237656565427929453	255.69417	78.86272	2.40	10.25	2104	1726	22.191	157	257	AGN
1237663269868994787	256.61725	78.82067	2.46	10.25	927	427	21.835	158	257	SF
1237656565427929429	255.55050	78.85917	2.51	10.25	1364	847	22.003	162	257	SF
1237656565427929436	255.39342	78.84628	2.56	10.25	631	463	21.668	163	257	SF
1237663269868994741	256.38988	78.85464	2.56	10.25	4175	2969	22.489	163	257	SF
1237663230678794779	257.04629	78.65342	2.85	4.87	40	27	20.470	172	211	ext
1237656565427929475	255.08483	78.81061	2.84	5.61	49	19	20.558	170	220	comp

Continued on next page

Table A.2 – *Continued from previous page*

SDSS ID	**RA** (degree)	**DEC** (degree)	**Area**$_{enc}$ (Mpc^2)	**Area**$_{obs}$ (Mpc^2)	**flux** (μ**Jy**)	**flux**$_p$ (μ**Jy**)	**log(lum)** (**W/Hz**)	**N**$_{enc}$	**N**$_{obs}$	**radio morphology**
1237656565427929441	255.10654	78.82394	2.99	10.25	231	147	21.232	176	257	comp
1237663230678794662	256.81508	78.50219	3.40	10.25	1200	643	21.947	182	257	SF
1237663231215665398	256.05950	78.91006	3.54	10.25	203	102	21.176	186	257	comp
1237663230678794725	257.01250	78.54406	3.58	9.10	109	70	20.906	187	253	ext
1237656565427929379	255.56883	78.90294	3.59	10.25	220	987	21.211	188	257	ext
1237655749380800875	254.90550	78.49481	4.18	8.46	98	66	20.859	198	246	comp
1237655749380735063	254.58692	78.72347	4.29	8.95	106	102	20.894	200	252	comp
1237663269332058258	256.63942	78.42208	4.70	7.05	63	50	20.668	206	236	comp
1237663269332058626	256.54883	78.41042	4.76	10.25	312	86	21.362	208	257	ext
1237663230678794417	257.13917	78.49839	5.05	10.25	3295	3225	22.386	214	257	AGN
1237663269869060123	257.24162	78.83753	5.58	10.25	892	174	21.819	219	257	AGN
1237656565427929306	255.13408	78.93606	5.70	10.25	255	217	21.275	222	257	comp
1237663230678794786	257.33050	78.50450	6.08	8.24	89	74	20.818	229	246	ext
1237656565428191416	255.85504	78.34411	6.16	10.25	828	306	21.786	230	257	SF
1237663230678859802	257.43850	78.51861	6.54	10.25	130	121	20.982	232	257	comp
1237656565428060410	255.78988	78.68897	0.08	5.33	43	26	20.509	11	218	comp
1237663231215665231	256.16165	78.88676	2.98	10.25	1032	378	21.882	176	257	comp
1237663231215599942	255.45625	79.03778	8.63	10.25	3165	2954	22.369	248	257	AGN
1237663269868994834	256.97933	78.74714	2.87	8.05	79	53	20.770	173	244	comp
1237663230678860038	257.41612	78.55214	5.85	10.25	356	54	21.420	224	257	ext
1237663230678794278	256.70400	78.59272	1.69	4.44	37	27	20.439	134	202	ext
1237663269868994760	256.75800	78.69140	1.59	10.25	251	160	21.269	130	257	ext
1237655749380800577	254.50925	78.56339	5.28	10.25	214	461	21.200	217	257	ext

Continued on next page

Table A.2 – *Continued from previous page*

SDSS ID	**RA** (degree)	**DEC** (degree)	**Area**$_{enc}$ (Mpc^2)	**Area**$_{obs}$ (Mpc^2)	**flux** (μ**Jy**)	**flux**$_p$ (μ**Jy**)	**log(lum)** (**W/Hz**)	**N**$_{enc}$	**N**$_{obs}$	**radio morphology**
1237656565427995115	255.33471	78.75531	1.27	5.56	47	24	20.544	111	219	comp
1237656565427863896	255.04458	79.00444	8.48	10.25	350	309	21.413	247	257	comp
1237656565427864068	254.95417	78.97222	7.63	10.25	295	106	21.339	243	257	ext
1237663269869060336	257.29125	78.87556	6.72	10.25	1860	370	22.138	234	257	SF
1237663269868929419	256.14958	78.66806	0.11	10.25	124	114	20.962	16	257	comp
1237663269868929423	255.90917	78.78278	0.80	10.25	132	43	20.991	87	257	comp
1237655749380669721	254.19667	78.78306	7.59	10.25	231	125	21.233	241	257	comp
1237655749380800829	254.71417	78.51667	4.75	10.25	330	105	21.387	207	257	comp
1237663269332189441	257.63000	78.48611	8.61	10.25	300	168	21.346	247	257	comp
1237663269332123864	257.19833	78.43222	6.98	10.25	192	58	21.153	235	257	ext
1237663269332123998	257.17417	78.39583	7.93	10.25	280	172	21.316	243	257	comp
1237655749380931763	255.53042	78.29167	8.68	10.25	322	119	21.377	250	257	comp
1237663230678794711	256.78229	78.64281	1.69	3.06	24	21	20.250	133	179	comp
1237656565428060463	255.89875	78.66500	0.00	1.45	19	18	20.150	1	121	comp
1237656565428061022	255.95204	78.64570	0.03	3.16	25	19	20.266	6	180	comp
1237663269868929212	256.28583	78.68500	0.31	10.25	1128	1107	21.921	48	257	comp
1237663269332123887	257.34125	78.36833	9.90	10.25	644	350	21.678	256	257	comp

[a:] The last two sources are not consider for statistical analysis because the optical and radio nuclei are not exactly match. These two sources are potential cluster radio galaxies

[b:] The Radio morphology classes are defined as follow: (ext) extended sources ,(ext(SF)) sources that are extended and the spiral alarms are so clear in optical image in addition to the radio emission that extended over the same area of optical emission, (SF) classified from Miller et al. [2003b] as a star forming galaxy ,(AGN) classified from Miller et al. [2003b] as a AGN.